Stabilization of the Li3PS4/Li interface by a 4 nm Al2O3 coating studied by in situ HAXPES

Lucía Pérez Ramírez, Jonas Sottmann, Benjamin Hennequart, Muath Radi, Maxime Hallot, Christophe Lethien, Lenart Dudy, Jean-Pascal Rueff, Rémi Dedryvère

Materials Today Communications 53 (2026) 115388

Contents lists available at ScienceDirect

Materials Today Communications

journal homepage: www.elsevier.com/locate/mtcomm

Stabilization of the Li_3PS_4/Li interface by a 4 nm Al_2O_3 coating studied by *in situ* HAXPES

Lucía Pérez Ramírez [a,b], Jonas Sottmann [a,b,1], Benjamin Hennequart [c], Muath Radi [d], Maxime Hallot [e,f,g], Christophe Lethien [e,f,g,h,*], Lenart Dudy [b], Jean-Pascal Rueff [b,i], Rémi Dedryvère [d,f,**]

[a] Sorbonne Université, CNRS, Physicochimie des Electrolytes et Nanosystèmes Interfaciaux, UMR 8234, 4 place Jussieu, Paris 75005, France
[b] Synchrotron SOLEIL, L'Orme des Merisiers, Saint-Aubin - BP 4891192 CEDEX, Gif-sur-Yvette, France
[c] Collège de France, Chaire de Chimie du Solide et de l'Energie, UMR 8260, 11 place Marcelin Berthelot, Cedex 05, Paris 75231, France
[d] IPREM, E2S-UPPA, CNRS, University of Pau & Pays Adour, Pau 64000, France
[e] Institut d'Electronique, de Microélectronique et de Nanotechnologies, Université de Lille, CNRS, Université Polytechnique Hauts-de-France, UMR 8520 - IEMN, Lille F-59000, France
[f] Réseau sur le Stockage Electrochimique de l'Energie (RS2E), FR CNRS 3459, France
[g] VOLTIFY, Avenue Henri Poincaré, Villeneuve d'Ascq 59650, France
[h] Institut Universitaire de France (IUF), Saint-Michel 103, Paris 75005, France
[i] Sorbonne Université, CNRS, Laboratoire de Chimie Physique Matière et Rayonnement, UMR 7614, 4 place Jussieu, Paris 75005, France

ARTICLE INFO

Dataset link: In situ HAXPES Al2O3 Li3PS4

Keywords:
In situ HAXPES
All-solid-state batteries
Lithium-metal
Li_3PS_4
Al_2O_3
ALD

ABSTRACT

Li-metal based All-Solid-State Batteries (ASSBs) offer a safer and higher-energy alternative to conventional lithium-ion batteries, but their performances are hindered by interfacial instability between the solid-state electrolyte (SSE) and lithium metal electrode. To stabilize the interface, a nanometer-thick Al_2O_3 film made by Atomic Layer Deposition (ALD) technique is evaluated as a surface protective layer at the SSE/Li metal interface. We unveil the interfacial stability between β-Li_3PS_4 (LPS) SSE and deposited lithium metal using *in situ* hard X-ray photoemission spectroscopy (HAXPES) approach. Our results on LPS/Al_2O_3/Li metal system reveal that 4 nm-thick Al_2O_3 coating enhances interfacial stability by mitigating undesirable side reactions. Although some LPS reduction to Li_2S still occurs, it is significantly less pronounced as compared to the pristine LPS/Li metal interface. Additionally, metallic lithium deposition is detected on the surface, with no observable reduction of phosphorus element. These findings underscore the capability of ultrathin oxide coatings made by ALD to significantly stabilize Li/SSE interface thus contributing to the development of more reliable and safety Li-metal based ASSBs.

1. Introduction

Li-ion batteries (LiBs) have dominated the battery market since they were commercialized for the first time in 1991. Their relatively high energy density, fast charging time and large lifespan allow for a wide range of applications, especially in portable electronics. However, accelerated technological progress has come along with new demands, such as electric transportation, which have propelled the search for greater energy density storage options. Actually, classical LiBs face two important issues: *(i)* a fire hazard associated with the use of organic liquid electrolytes, and *(ii)* their limited power and energy densities for demanding new applications, such as electric transportation [1]. The latter limitation can be overcome if metallic lithium is used as the negative electrode, instead of lithiated graphite. Its very high specific capacity (3860 $mAh.g^{-1}$) and low operating potential allows for higher energy densities [2]. Nevertheless, the metallic lithium electrode is prone to form dendrites during repeated charge-discharge cycles, which induce capacity loss of the battery and severe safety concerns [1].

* Corresponding author at: Institut d'Electronique, de Microélectronique et de Nanotechnologies, Université de Lille, CNRS, Université Polytechnique Hauts-de-France, UMR 8520 - IEMN, Lille F-59000, France
** Corresponding author at: IPREM, E2S-UPPA, CNRS, University of Pau & Pays Adour, Pau 64000, France.
E-mail addresses: christophe.lethien@univ-lille.fr (C. Lethien), remi.dedryvere@univ-pau.fr (R. Dedryvère).
[1] Equinor AS, Martin Linges vei 33, NO-1364 Fornebu, Norway

https://doi.org/10.1016/j.mtcomm.2026.115388
Received 25 February 2026; Received in revised form 30 April 2026; Accepted 13 May 2026
Available online 15 May 2026

Li based All solid-state batteries (ASSBs) have emerged as a suitable alternative to traditional LiBs given their ability to solve the above-mentioned issues. First, they address the safety issues of LiBs by replacing the liquid flammable electrolyte with a solid-state electrolyte (SSE). Second, since the SSE serves as an electrode separator itself, it is a better physical barrier against dendrite propagation than classical porous separators used with liquid electrolytes. This enables the use of metallic Li as negative electrode in ASSB, resulting in higher energy densities of batteries [3,4]. The generally low ionic conductivity of common SSE materials had been formerly seen as the major constraint for the development of ASSBs, but this has been dealt with by using new generations of Li-ion conductors. Sulfide-based materials were found to exhibit the highest room-temperature ionic conductivities among Li-ion conductors. With ionic conductivity values of $\sim 10^{-2}$ S cm^{-1} at room temperature, lithium thiophosphates can compete with their liquid organic electrolyte contenders [5–7]. Among them, β-Li_3PS_4 (called LPS hereafter) has caught particular attention not only due to its high conductivity ($\approx$ 0.15 mS cm^{-1}), but also to its convenient mechanical properties for easy battery processing [8].

However, ASSB technology still suffers from the impossibility of building chemically stable interfaces between the SSE and the Li-metal electrode [9,10]. Few SSEs, like garnet-type materials, are chemically stable towards Li but suffer from a large interfacial resistance when in contact with it. Many other ones, especially sulfide-based materials (including the argyrodite family), are not thermodynamically stable against Li metal and undergo a extensive decomposition when in contact with it [9]. Ideally, the degradation should be self-limiting and form a metastable ionically conducting and electronically insulating solid electrolyte interphase (SEI) layer on the Li metal, comparable to the one formed in classical LiBs on lithiated graphite electrode when using liquid electrolytes. In most cases, however, it forms a mixed-conducting interphase (which simultaneously conducts electrons and Li^+ ions) which may grow into the solid electrolyte and alter the properties of the whole bulk material due to a continuous decomposition [11,12]. This induces capacity degradation, ultimately affecting long-term battery cycling performance, as it is shown by the rise in impedance with contact time (a consequence of a higher interfacial resistance and, thus, a lower Columbic efficiency) [13]. In the worst case, the SEI layer will keep growing until a short-circuit occurs.

Attempts to stabilize the interface between the SSEs and metallic lithium electrode in ASSB are mainly based on the deposition/growth of nanometer-thick stable coatings or the formation of stable passivation layers at the Li/SSE interface to generate artificial SEIs [14]. To reach this goal, the deposited/grown artificial SEI could be an insulating layer (Al_2O_3, ZnO…) or a thin film solid ionic conductor ($LiNbO_3$, Li_3PO_4, Li_2ZrO_3…) [15–17] that allows Li conduction through the artificial layer while stabilizing the chemistry at the SSE/Li interface. In general, these interfacial coatings help to establish more homogeneous interfaces between the Li metal electrode and the SSE, by improving physical contact (which favors an even current distribution), stabilizing the surface chemistry and reducing stress [18]. This strategy appears to be effective for garnet-type electrolytes used in ASSB, as it has been observed that a thin oxide layer (Al_2O_3) made by solution processing route on LLZO decreases interfacial resistance, suppresses Li dendrite formation, and improves capacity retention of the battery [19]. The use of several mixtures of metallic alloys as protective coatings exhibits similar beneficial effects [20].

The coating strategy has also been used for stabilizing the interface between thermodynamically unstable SSEs (such as sulfides, argyrodites, halides) and lithium metal electrode. It appears that a thin metal M (for example indium) layer between a Li_2S-P_2S_5 solid electrolyte and Li metal can increase the capacity retention of a battery [14,21]. This is explained by the formation of a LiM-alloy phase with a higher working potential than pure Li, hence limiting the chemical reduction of the SSE. Nonetheless, this greater working potential of the negative electrode ultimately means a lower cell voltage and, thus, a lower energy density of the battery. Hence, other types of coatings such as insulating metal oxide layer or ionic conducting film still need to be explored. In any case, a fundamental understanding of the chemical stability of SSE/protective coating/Li interfaces is necessary for further development of high-performance ASSBs for practical applications. However, the non-destructive characterisation of these buried interfaces is not an easy task and has been very much limited to phenomenological techniques such as cyclic voltammetry (CV) or electrochemical impedance spectroscopy (EIS), both being not chemically specific methods. X-ray photoelectron spectroscopy (XPS) is one of the best experimental characterization methods to probe the chemical composition of interfaces. However, it is limited by its probing depth of a few nanometers (with classical laboratory X-ray sources) and thus raises the problem of non-destructive characterization of buried interfaces. To reach this goal, a relevant approach consists in depositing a Li metal film using Physical Vapour Deposition (PVD) techniques at the surface of the SSE, and following the evolution of the surface chemistry by XPS *vs.* the deposited thickness and step of the thin film growth (nucleation, coalescence, grain growth). In an effort to chemically identify the reaction products formed at the Li/SSE metal interface, Wenzel *et al.* conceived an *in situ* XPS experiment combined with time-resolved EIS and have reported results for several sulfide-based solid electrolytes [12], including $Li_{10}GeP_2S_{12}$ [22], $Li_7P_3S_{11}$ [23], and argyrodite Li_6PS_5X (X = Cl, Br, I) [24]. They carried out the Li deposition by focusing the argon ion gun (commonly available in the XPS analysis chamber) onto a metallic Li foil to sputter off and deposit Li onto the adjacent SSE. Several deposition and measurement cycles could be done sequentially, which allowed them to follow the reaction at several steps, and revealed the S 2p and P 2p fingerprints of Li_3P and Li_2S reduced species at the SSE / Li interface. The presence of these phases degrades the interfacial properties between the SSE and lithium, as demonstrated by the increasing of the charge transfer resistance over deposition time. This observation, again, stresses the need for interface modification, *e.g.* using a protective coating, to grant the formation of a stable and low-impedance interphase in between a highly reactive SSE (such as sulfide-based SSE) and Li metal electrode.

However, the method consisting in Li deposition on the SSE by using argon ion sputtering on a metallic Li foil leads also to the deposition of impurities due to the initial surface state of the metallic Li foil, which always contains native oxide, hydroxide and carbonate, thus disturbing the analysis of the created Li/SSE interface. Moreover, it has been shown that the energetic incident Li atoms deposited by this method may cause beam damage and change the chemical nature of species at the surface of a sulfide SSE [25]. Another method, sometimes called quasi-electrochemical deposition, consists in plating metallic Li *in situ* using an electron beam via the XPS electron flood gun to induce a negative charge accumulation on the SSE surface, with the SSE pellet placed on a lithium counter electrode. This negative surface charge electrochemically reduces Li^+ ions into metallic Li at the surface of the SSE facing the XPS analyzer [26,27]. Interestingly, Gibson *et al.* [21] observed that this method is also prone to induce slight beam degradation due to the ill-favored formation of an oxygen deficient interface, and recommended the use of Li thermal evaporation instead, although they could not avoid the formation of Li_2O and LiOH by this evaporation method.

A last method, originally used with oxide-based SSEs [28], consists in using a dedicated lithium getter connected to the XPS analysis chamber, which produces Li vapor by reduction of a lithium salt. This method avoids pollution by the native oxide/hydroxide/carbonate layer at the surface of metallic lithium, and so we adopted this approach in this work.

Herein we develop a methodology to study the stability of SSE / Li interface by: *(i)* protecting the Li_3PS_4 (LPS) based SSE pellet with a nanometer-thick Al_2O_3 layer made by Atomic Layer Deposition (ALD) method, *(ii)* depositing Li metal on bare and coated LPS pellets *in situ* within the analysis chamber following the method proposed by

Schwöbel *et al.*, [28] and *(iii)* studying the surface chemistry by Hard X-ray PhotoEmission Spectroscopy (HAXPES). Thanks to higher photon energies produced at synchrotron, HAXPES provides a larger probing depth compared to classical XPS and thus is less dependent on the possible surface pollutions (we have used photons of 2300 eV instead of 1487 eV produced by common laboratory X-ray sources). By investigating buried LPS/Li and LPS/Al_2O_3/Li interfaces, we demonstrate how a ultra-thin Al_2O_3 layer enhances the stability of a sulfide-based SSE towards metallic lithium.

2. Experimental

2.1. Preparation of the SSE samples

β-Li_3PS_4 (LPS) was prepared as described previously in the literature [29]. Briefly, a solvent-mediated synthesis was carried out by reacting stoichiometric amounts of Li_2S and P_2S_5 in THF for 48 h at room temperature. The resulting powder was then recovered and thoroughly dried before use.

The lithium-indium/LPS composite was prepared in a two-step process. First, Li and In foils were weighed to achieve a $Li_{0.8}In$ stoichiometry and then laminated and folded together until the resulting alloy became a brittle dull grey metal. Subsequently, the obtained alloy was mixed with LPS in a LiIn:SSE = 60:40 wt ratio in an agate mortar, until a homogeneous powder was obtained.

The studied samples were 13 mm diameter bilayer pellets comprising a top layer of pure LPS and a bottom layer of $Li_{0.8}In$/LPS composite. This bottom layer helped to ensure electrical contact with the sample holder and thus minimize charging effects during the HAXPES measurements.

2.2. Preparation of the surface protective layer by ALD method

The LPS pellets were coated with a 4 nm-thick Al_2O_3 film made by Atomic Layer Deposition (ALD). Several LPS samples were not coated to be used as bare reference samples.

The ALD process of Al_2O_3 films was performed in a PicoSun R200 advanced reactor. The Al_2O_3 layer was deposited on the top of LPS pellet samples by ALD operating in thermal ALD mode using Trimethylaluminum (TMA) and O_3 (ozone). The ozone generation is achieved by corona discharge ozone generating technology based on O_2 (99.5%) / N_2 (0.5%) mixing gaz. To control the thickness at the atomic level, the deposition parameters such as reactor temperature, time duration of the TMA precursors and O_3 reactant and number of ALD cycles was carefully investigated on silicon substrate. The duration of the purge step is fixed at 5 s. The Growth per Cycle (GPC) of the Al_2O_3 process is then evaluated and the number of ALD cycles is tuned to reach the targeted thickness (4 nm) on LPS pellets. After optimization, the ALD process was done at 150 °C.

2.3. *In situ* *metallic lithium deposition*

Deposition of metallic lithium on the SSE pellets surface was carried out by production of a pure lithium vapor through a lithium metal dispenser (SAES Getters Group), by reduction of lithium chromate Li_2CrO_4 via a reducing agent (Zr 84% - Al 16% alloy). The Zr agent also sorbs the chemically active gases produced during the reduction reaction, preventing them from contaminating the lithium vapor. Resistive heating was applied to the dispenser in the HAXPES analysis chamber to start the Li deposition.

The composition of the residual gas in the analysis chamber during the Li evaporation was followed by a RGA MKS LM92 Microvision mass spectrometer.

2.4. HAXPES measurement

HAXPES measurements were carried out on GALAXIES beamline at Synchrotron SOLEIL [30]. The spectra were collected at a photon energy of 2.3 keV (λ = 5.39064 Å), which allowed for a probing depth of ~14 nm in LPS for Li 1 s, P 2p and S 2p core peaks (and ~23 nm in metallic lithium for Li 1 s core peak) [31]. The spot size was 30 × 80 mm^2 (V×H). Sample handling and transfer to the HAXPES chamber was always performed under inert gas atmosphere (Ar) using a dedicated, compact UHV chamber which be transported from the SOLEIL glove box to the samples load lock. All measurements were done at room temperature. Lithium deposition and HAXPES data acquisition were performed at alternated steps. An image of the pellet on its sample holder and of the deposition setup is shown in the supporting information (SI) in Figure S1. The chamber pressure was ~10^{-8} mbar during the HAXPES measurements.

Two LPS pellets (Al_2O_3-coated and bare reference sample) were investigated on the same sample plate and during the same run, which ensured a uniform deposition process for sample comparison. Along with the two pellets, a small piece of metallic copper was stuck on the sample plate to serve as a reference to estimate the thickness of the deposited metallic Li layer, using the Cu 3p core peak (the method is described as supplementary information, see Figures S2, S3 and accompanying text). Data analysis was performed using Global Fit method of Igor Pro.

3. Results and discussion

3.1. ALD process optimization for Al_2O_3 surface protective layer

The study, described in Fig. 1a, starts with the optimization of the coating process to stabilize the LPS / Li metal interface against the formation of undesired by product issued from the instability of the interface (Fig. 1b). The growth per cycle (GPC), *i.e.* the deposition rate, is evaluated with the temperature of the ALD reactor because we do not want to modify the properties of the LPS samples if the deposition of the surface protective layer is made at high temperature. Moreover, the ALD process has to be achieved in a temperature range where the GPC is stable and do not depend on the temperature to get the best ALD conditions. The Fig. 1c describes how the GPC is modified vs the temperature of the reactor while keeping fixed the other deposition parameters (t_{TMA}, $t_{03,}$ t_{purge} and number of ALD cycles): non surprisingly, the GPC of the Al_2O_3 layer (TMA / O_3) is stable between 100 and 350 °C. We thus fix the temperature at 200 °C (in the middle of the temperature range) for studying the effect of other deposition parameters onto the saturation plots.

The duration of the TMA pulse (t_{TMA}) is then tuned and we observe that the GPC is stable once the t_{TMA} is higher than 0.1 s (Fig. 1c). Similar trend is observed for the time duration of the ozone pulse (stability if t_{O3} is higher than 0.1 s). Finally, we decide to evaluate how the thickness of the Al_2O_3 film can vary vs the number of ALD cycles within the temperature range where we can observe stable GPC (between 100 and 350 °C). The plot reported in Fig. 1d shows the quasi-linear relationship in between the thickness and the number of ALD cycles. The GPC (slope of the plots) moves from 0.53, 0.67 and 0.74 Å per cycle when the temperature reaches 100, 200 or 300 °C respectively. The higher the temperature, the higher the GPC is. In order not to modify the properties of SSE LPS pellets and to form a dense Al_2O_3 coating, we thus decide to fix the temperature of the ALD process (TMA / O_3) close to 150 °C. Based on this temperature, we prepare various LPS samples coated with Al_2O_3 film having different thicknesses (from 1 up to 10 nm). A 4 nm-thick Al_2O_3 film represents an optimal compromise between chemical protection (providing a pinhole-free, protective layer) and efficient ion conduction at the nanoscale. Increasing the film thickness leads to a limitation in lithium ion transport through the Al_2O_3 dielectric layer. Decreasing the thickness does not prevent chemical reactions with metallic lithium. At 150 °C, the GPC is ~ 0.6 Å.$cycle^{-1}$ meaning that ~ 67 ALD cycles is sufficient to reach the targeted thickness (4 nm). The second step of the study consists in evaluating the properties of the bare

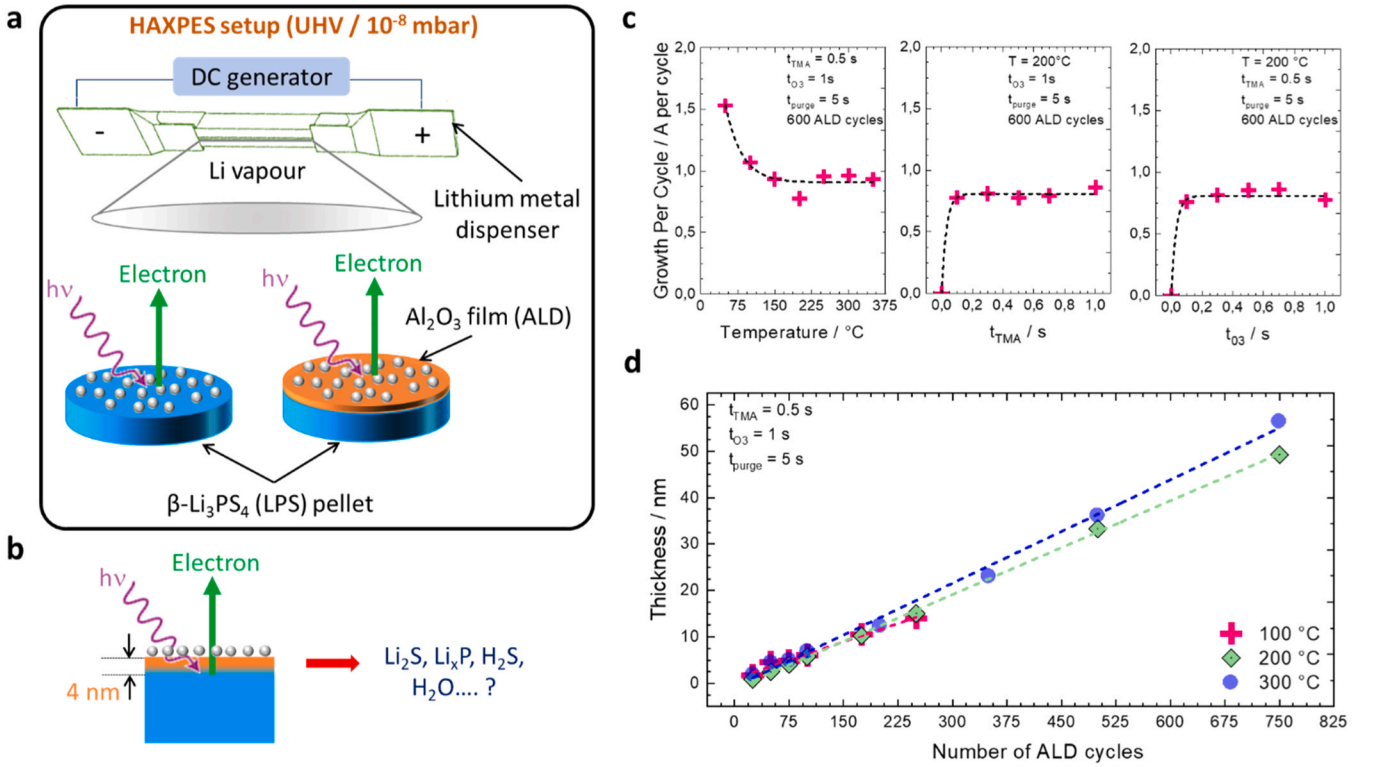

Fig. 1. Overview of the proposed study and test setup used to monitor the β-Li_3PS_4 (LPS) / Li metal interface. Bare LPS pellet and protected LPS one with an Al_2O_3 surface protective layer made by Atomic Layer Deposition (ALD) are carefully studied. **(a)** HAXPES setup installed in the GALAXIES beamline at Soleil synchrotron. The setup includes an alkali metal dispenser to evaporate Li metal on fresh & coated LPS pellets. **(b)** Schematic illustrating the role of the Al_2O_3 coating layer to stabilize the LPS/Li metal interface. **(c)** Growth per cycle plots of the Al_2O_3 film *vs.* the deposition parameters (temperature of the ALD reactor, time duration of the TMA precursor, time duration of the ozone reactant) while keeping fixed the number of ALD cycles (600 cycles) and the t_{purge}. **(d)** Evolution of the thickness of the Al_2O_3 layer made at 100, 200 and 300 °C *vs.* the number of ALD cycles.

and coated LPS pellets by *in situ* HAXPES.

3.2. Study of the bare Li_3PS_4 pellet

Fig. 2 depicts the HAXPES O 1 s, S 2p, P 2p and Li 1 s spectra of the pristine uncoated LPS pellet and their evolution as a function of the amount of deposited Li. The evolution of C 1 s spectra is also shown in Figure S4a.

The characteristic signature of pristine LPS appears systematically in the S 2p ($2p_{3/2}$ component at 161.5 eV), P 2p ($2p_{3/2}$ component at 132.0 eV) and Li 1 s (55.4–55.7 eV) spectra. The binding energy values correspond well to what has already been reported in the literature for LPS and other thiophosphate SSEs [20,32–34]. In the S 2p and P 2p spectra, weak doublets are also observed at + 1 eV binding energy, which can be assigned to small traces of P_2S_x [31], but no trace of surface oxidation of LPS can be evidenced, since the characteristic signatures of sulfites and sulfates (S $2p_{3/2}$ component at ~167 eV and ~169 eV, respectively) or phosphates (P $2p_{3/2}$ at ~134 eV) cannot be detected. The presence of weak peaks in the O 1 s spectrum can be explained by the existence of adsorbed carbonaceous species at the surface (CO and COO environments of carbon, which is confirmed by the C 1 s spectrum, see Figure S4a).

The evolution of the surface chemistry can be observed in panels **(b-e)** of Fig. 2. Each of the panels is annotated with the estimated deposited layer thickness (see Figures S2, S3 and accompanying text in SI for calculation details). The visible changes in all core peaks indicate that significant chemical changes occur right from the first evaporation cycle, as shown by panel **(b)**. First of all, no characteristic signature of metallic lithium in the Li 1 s spectra (thin peak expected at ~52–53 eV) can be detected, even after long deposition time, which means that the deposited Li immediately reacts with the surface to form new products. Moreover, it is evident from the observation of S 2p and P 2p spectra that LPS is rapidly converted into Li_2S (S $2p_{3/2}$ component at ~160.0–160.5 eV) and phosphides Li_xP (P $2p_{3/2}$ component at binding energies $\leq$ 130 eV). From the curve fitting, four different kinds of phosphides are successively formed, with Li_3P (P $2p_{3/2}$ at ~126 eV) being the final reduction product for the greatest Li deposition amounts [19,35,36]. After deposition of a ~7.9 nm thick layer at the surface, the original S 2p and P 2p signatures of LPS become minority peaks, which means that LPS is converted into the most reduced species as possible (Li_2S and Li_3P), which can be summarized as $Li_3PS_4 + 8Li \rightarrow 4Li_2S + Li_3P$, and reveals its extremely high reactivity towards metallic Li. Please note that evaporated lithium may be more reactive than a lithium foil in contact with LPS powder, as used in real battery conditions. However, this experiment shows that LPS is not stable towards Li.

Besides, despite the relative increase of the reduction species with respect to the main LPS component, both the S 2p and P 2p core peaks get globally attenuated as deposition occurs, which may indicate a top overlayer. A look onto the O 1 s spectra reveals that additional oxygenated subproducts are formed on the surface. Contrary to the attenuated S 2p and P 2p spectra, the O 1 s intensity increases with further Li evaporation. A characteristic O 1 s signature at extremely low binding energy (528.2 eV) corresponds to a very negatively charged O^{2-} anion and can be unequivocally assigned to Li_2O [37], whose formation is presumed to be caused by the residual oxygen and water in the analysis chamber, this even though the chamber has been subjected to a bakeout process before the experiment and is kept at ultra-high vacuum during the measurements. An additional O 1 s component appears at slightly higher binding energy (530.6 eV), which is in good agreement with the formation of LiOH [33]. The formation of LiOH could result from chemical reaction of evaporated Li with traces of gaseous water in the chamber. To complement this qualitative analysis of photoemission

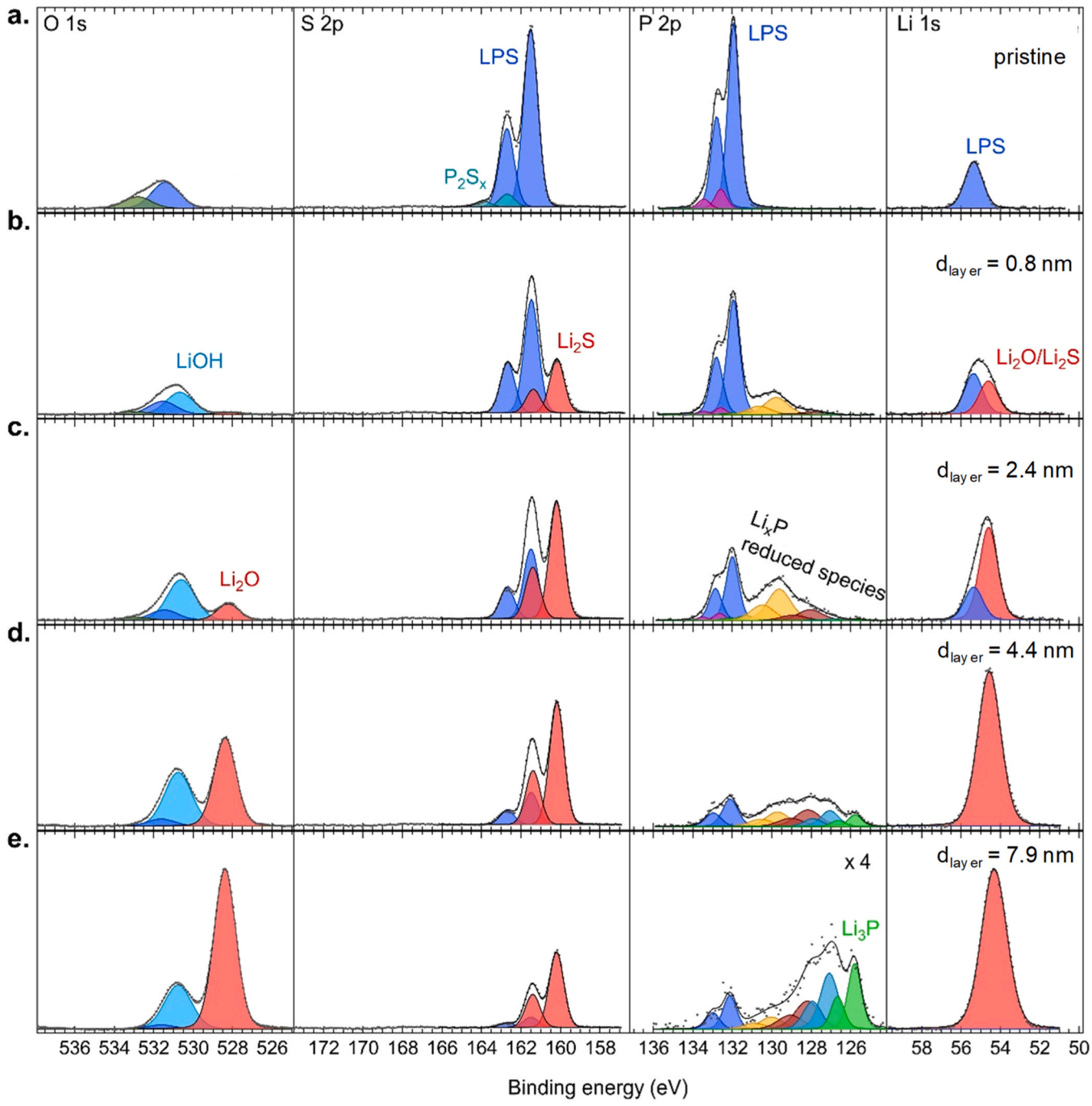

Fig. 2. HAXPES O 1 s, S 2p, P 2p and Li 1 s spectra of: **(a)** the pristine uncoated LPS pellet, and **(b-e)** at different steps of lithium deposition, with estimated deposited layer thickness (see SI for more details).

spectra, we have included in Table 1 the relative atomic percentages corresponding to all identified compounds for sulfur, phosphorus, lithium and oxygen as a function of the estimated deposited lithium layer thickness. Note that, due to the lack of knowledge of the analyzer's transmission function at all possible photon energies, it is not possible to draw a general chemical composition of the surface as it is commonly done with XPS machines working at fixed photon energy. Therefore, only the relative at% for each element are given.

Additionally, the evolution of C 1 s spectrum (Figure S4a) does not evidence the formation of any carbonate species (like Li_2CO_3, expected at ~290 eV), but interestingly reveals the partial reduction of some carbonaceous species adsorbed at the surface into lithium carbide Li_xC (very low C 1 s binding energy at ~282–283 eV). To get more insight into the possible side reactions occurring during the Li evaporation process, we have followed the composition of the residual gas in the analysis chamber during and between the successive evaporation steps by mass spectrometry, as shown in Figure S5. This analysis reveals the continuous presence of residual O_2, H_2O and H_2S, whose partial pressure slightly increases during each Li evaporation cycle, and decreases at the end of the cycle. The presence of O_2 and H_2O explains the formation of Li_2O and LiOH at the surface. The presence of H_2S certainly results from the reaction between H_2O and LPS, a reaction that sulfide SSEs are known to undergo [38], and H_2S may slightly contribute to the formation of Li_2S, besides the main reaction of evaporated Li with LPS. As a conclusion, this experimental approach allows to describe precisely the degradation mechanisms of uncoated LPS with Li, although side

Table 1
Relative atomic percentages corresponding to all compounds identified in Fig. 2 (uncoated LPS pellet) for sulfur, phosphorus, lithium and oxygen as a function of the estimated deposited lithium layer thickness.

Relative at% for each element		d_{layer} (nm)				
		0 (pristine)	0.8	2.4	4.4	7.9
Sulfur	Li_3PS_4	94.7	64.7	34.5	18.5	9.6
	Li_2S	—	34.7	64.5	81.5	90.4
	P_2S_x	4.2	—	—	—	—
	SO_3	1.1	0.6	—	—	—
Phosphorus	Li_3PS_4	88.2	65.0	47.8	27.5	14.5
	Li_xP	—	29.5	52.2	72.5	85.5
	P_2S_x	11.8	5.5	—	—	—
Lithium	Li_3PS_4	100	51.4	24.5	—	—
	Li_2O/Li_2S	—	48.6	75.5	100	100
Oxygen	Surface O	100	37.8	24.2	4.2	2.8
	LiOH	—	56.8	56.2	43.7	26.2
	Li_2O	—	5.4	19.6	52.0	71.0

products cannot be avoided.

3.3. New insights on the interface stability of the Al_2O_3-coated Li_3PS_4 pellet

Fig. 3 displays the HAXPES O 1 s, S 2p, P 2p, Al 2p and Li 1 s spectra of the pristine LPS pellet coated with 4 nm-thick Al_2O_3 layer, and the evolution of these spectra after metallic Li deposition. The evolution of C 1 s spectra is also shown in Figure S4b.

The presence of the Al_2O_3 coating in the pristine sample is confirmed by an Al 2p doublet ($2p_{3/2}$ component at 74.9 eV) and a large O 1 s component at 532.4 eV dominating the O 1 s spectrum [39]. The characteristic peaks of LPS are still detected (*i.e.*, the S $2p_{3/2}$ peak at 161.5 eV and P $2p_{3/2}$ peak at 132.0 eV), due to the thinness of the coating (which is lower than the HAXPES probing depth). One striking difference between the uncoated and Al_2O_3-coated LPS samples is related to the surface oxidation of the samples. While the uncoated LPS pellet appears almost devoid of surface oxidation, the coated sample with Al_2O_3 film has a considerable quantity of sulfate SO_4 (S $2p_{3/2}$ component at 169.5 eV) and sulfite SO_3 (S $2p_{3/2}$ component at 167.5 eV), as well as phosphate PO_4 (P $2p_{3/2}$ components at ~134 eV) and partially oxidized thiophosphate $PO_{4-x}S_x$ (P $2p_{3/2}$ component at ~133 eV). One should expect to detect corresponding signals for these oxygenated species in the O 1 s spectrum, but they are masked by the broad O 1 s peak of alumina. The presence of these oxygenated species may be due to LPS

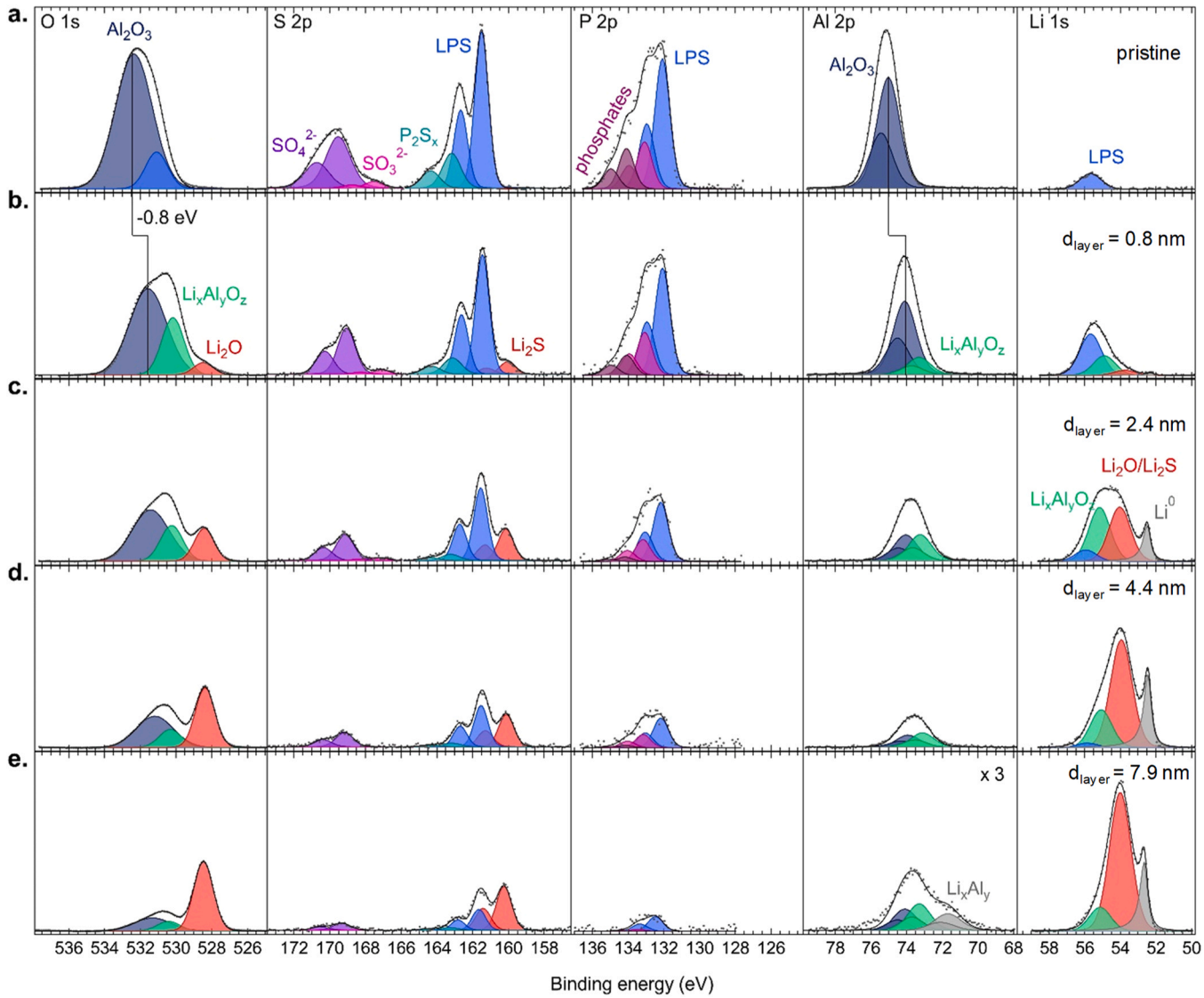

Fig. 3. XPS spectra of 4-nm Al_2O_3 coated LPS, (a) pristine (b-e) during lithium deposition, with estimated deposited layer thickness.

oxidation by ozone during the very first step of alumina deposition, and may stabilize the Al_2O_3/LPS interface during growing of the coating. Their presence may influence the interface impedance of the solid electrolyte. However, Al_2O_3 by itself has a very low ionic conductivity for Li^+ ion diffusion [40,41] and contributes to an interface impedance increase, but makes suitable coatings for solid electrolytes due to the very low deposited thicknesses [42,43]. Concerning phosphates and sulfates, although Li_2SO_4 and Li_3PO_4 have also poor ionic conductivities at room temperature, it was shown that glassy mixtures based on the Li_2SO_4-Li_2O-P_2O_5 ternary system display increased ionic conductivities compared to the components considered separately [44]. Moreover, Li_3PO_4 was already successfully used as surface coating for cathode materials ($LiNi_{0.5}Mn_{1.5}O_4$ for example) [16]. Therefore, we do not expect any detrimental effect of these surface oxidized species, whose thickness is lower than the Al_2O_3 coating itself.

Besides, Figure S4b shows the presence of carbonate at the surface, which is also different from the uncoated LPS.

The evolution of the protected LPS sample during lithium deposition is shown in Fig. 3(b) to (e). Note that when comparing panels (a), pristine, and (b), first deposition step, there is a marked shift towards lower binding energy (-0.8 eV) of some of the measured spectra, notably O 1 s and Al 2p, which are the ones assigned to Al_2O_3. This can be explained by an energy band alignment between the different interfaces, which has been well described in the past [45], following the deposition of a first thin metallic Li layer. There is no further shift during further lithium deposition cycles.

The deposition of a metallic lithium (Li^0) layer on the coated pellet is confirmed by the appearance of a very sharp characteristic Li 1 s peak at low binding energy (around 52.5 eV, grey in Fig. 3). To better take into account its metallic character, it has been fitted with an asymmetrical shape classically used for metallic conductors [46]. The successful deposition of a metallic Li layer already provides an important information regarding the chemical reactivity of the Al_2O_3-coated LPS SSE towards Li metal: contrary to what is observed for the uncoated LPS pellet, here the evaporated Li does not react immediately with the material, which allows its deposition at the surface as a metallic layer, and proves the decreased reactivity of Al_2O_3-coated LPS towards Li.

Although the surface of the pristine coated pellet is contaminated by oxidized species (sulphates and phosphates) resulting from the alumina ALD process (as mentioned earlier), their relative proportion to LPS remains reasonably constant over Li deposition time. Looking at the evolution of S 2p spectra, this sample also shows reduction of LPS into Li_2S during Li evaporation, as demonstrated by the increase of the red peak at ~160 eV, but to a much lesser extent compared to the uncoated LPS. To complement Fig. 3, we have also included in Table 2 the relative atomic percentages corresponding to all identified compounds for sulfur, phosphorus, lithium and oxygen as a function of the estimated deposited lithium layer thickness.

Table 2
Relative atomic percentages corresponding to all compounds identified in Fig. 3 (Al_2O_3 coated LPS pellet) for sulfur, phosphorus, lithium and oxygen as a function of the estimated deposited lithium layer thickness.

Relative at% for each element		d_{layer} (nm)				
		0 (pristine)	0.8	2.4	4.4	7.9
Sulfur	Li_3PS_4	50.6	54.3	48.6	41.8	31.2
	Li_2S	—	6.6	22.1	35.2	57.3
	P_2S_x	15.7	9.7	4.9	4.4	—
	SO_3	4.1	2.4	2.7	1.1	—
	SO_4	29.6	27.0	21.7	17.5	11.5
Phosphorus	Li_3PS_4	52.4	59.6	66	60	80
	Li_xP	—	—	—	—	—
	P_2S_x/PO_4	47.6	40.4	34	40	20
Lithium	Li_3PS_4	100	63.0	11.0	4.6	—
	Li_2O/Li_2S	—	9.2	38.9	59.7	71.2
	Li_xAlO_y	—	25.9	38.1	19.3	12.7
	Li^0	—	1.9	12.0	16.4	16.1
Oxygen	Al_2O_3	87.8	63.1	56.6	42.7	21.9
	Surface O	12.2	—	—	—	—
	Li_xAlO_y	—	31.5	23.4	15.1	11.5
	Li_2O	—	5.4	19.9	42.2	66.6

Moreover, no reduction products (Li_xP) are observed in the P 2p spectra. As it is difficult to imagine the reduction of LPS into Li_2S without its simultaneous reduction into Li_xP, this could be an indication that the formed Li_2S may not mainly originate from SSE degradation, but rather from reaction of the evaporated Li with residual H_2S in the chamber, as evidenced by mass spectrometry (Figure S5). Additionally, the formation of Li_2O is observed, which could result from the reaction of evaporated Li with residual oxygen or water in the chamber. It may also arise from the chemical interaction between the deposited Li and the Al_2O_3 coating. Indeed, compared to the uncoated LPS material, we observe the appearance of new components (green in Fig. 3) in O 1 s (at 530.2 eV), Al 2p (at 73.3 eV) and Li 1 s spectra (at 55.0 eV) that we have attributed to lithium aluminium oxide $Li_xAl_yO_z$. Actually, the reaction between alumina and metallic lithium has been reported earlier, and results in a variety of compounds including Li_9Al_4, Li_5AlO_4, and $LiAlO_2$ [47]. The formation of $LiAlO_2$ is in good agreement with the observed lower binding energies with respect to Al_2O_3, as already outlined by other authors [41,48,49]. Fig. 3e depicts a third component (grey) in Al 2p spectrum arising at the end of the experiment, during the last evaporation cycles. Its position matches well with what is expected for metallic Al, since it has a core-level shift of −2.4 eV with respect to alumina [36]. This leads us to the assumption that a Li_xAl_y phase is forming as well. It might be overlapped with the signal of metallic lithium in the Li 1 s spectrum. In this way, the Al_2O_3 coating made by ALD on LPS SSE could not only act as a chemical barrier, but may also have a partially sacrificial role in the protection of LPS against Li, although most of the coating still remains unreacted.

4. Conclusions

In this work, we have investigated the interfacial stability of β-Li_3PS_4 (LPS) solid electrolyte in contact with metallic lithium, focusing on the impact of a thin Al_2O_3 coating made by Atomic Layer Deposition method using TMA precursor and O_3 reactant at 150 °C. By using an *in situ* HAXPES approach, we have demonstrated that the presence of a 4 nm-thick Al_2O_3 surface protective layer significantly improves the stability of LPS versus lithium metal. For the uncoated LPS sample, Li deposition led to severe interfacial degradation, as evidenced by the formation of Li_2S and Li_xP species, along with a continuous reduction of phosphorus-containing species with further Li deposition. Within the probe volume, LPS was almost totally converted into these species. In contrast, the Al_2O_3-coated LPS sample exhibited a more stable interface upon lithium deposition. Although some formation of Li_2S was still observed, phosphorus reduction was largely suppressed, indicating that the alumina layer effectively mitigates the degradation of LPS. Furthermore, the presence of metallic lithium (Li^0) was confirmed on the coated sample, which suggests less reactivity between the SSE and Li. The formation of lithium aluminum oxide ($LiAlO_2$) and Li_xAl_y phases indicated an interaction between lithium and alumina, which may influence interfacial properties.

Overall, our findings highlight the importance of interface engineering in solid-state batteries, particularly through protective coatings like Al_2O_3 made by ALD, which can enhance the stability of sulfide-based solid electrolytes against lithium metal. Further optimization of coating materials and deposition techniques will be essential to achieve stable, low-resistance interfaces, which are critical for practically implementing all-solid-state lithium batteries.

CRediT authorship contribution statement

Lenart Dudy: Software, Methodology. **Christophe Lethien:** Supervision, Methodology, Conceptualization. **Benjamin Hennequart:**

Investigation. **Jonas Sottmann:** Funding acquisition, Conceptualization. **Maxime Hallot:** Methodology, Investigation. **Muath Radi:** Writing – review & editing, Investigation. **Lucía Pérez Ramírez:** Writing – original draft, Investigation, Data curation. **Rémi Dedryvère:** Writing – review & editing, Supervision, Conceptualization. **Jean-Pascal Rueff:** Validation, Investigation.

Declaration of Competing Interest

The authors declare that they have no known competing financial interests or personal relationships that could have appeared to influence the work reported in this paper.

Acknowledgments

Experiments were performed at the GALAXIES beamline at SOLEIL Synchrotron, France under Proposal #20211057. The authors acknowledge the French National Research Agency (ANR) for its support through Labex STORE-EX project (ANR-10LABX-76–01). MR, CL and RD acknowledge LIMASSE project (ANR-22-PEBA-0004) funded by France 2030 program. CL thanks the French RENATECH network and the University of Lille for supporting the Center of MicroNanoFabrication (CMNF) facility from IEMN. This work received funding from the CPER Hauts de France project IMITECH and MEL.

Appendix A. Supporting information

Supplementary data associated with this article can be found in the online version at doi:10.1016/j.mtcomm.2026.115388.

Data Availability

I have shared the link to my data at the attach file step
In situ HAXPES Al2O3 Li3PS4 (Cloud IPREM)

References

[1] N.-S. Choi, Z. Chen, S.A. Freunberger, X. Ji, Y.-K. Sun, K. Amine, G. Yushin, L. F. Nazar, J. Cho, P.G. Bruce, Challenges facing lithium batteries and electrical double-layer capacitors, Angew. Chem. Int. Ed. 51 (2012) 9994–10024, https://doi.org/10.1002/anie.201201429.
[2] J. Xie, Y.-C. Lu, A retrospective on lithium-ion batteries, Nat. Commun. 11 (1) (2020) 2499, https://doi.org/10.1038/s41467-020-16259-9.
[3] L. Wang, J. Li, G. Lu, W. Li, Q. Tao, C. Shi, H. Jin, G. Chen, S. Wang, Fundamentals of electrolytes for solid-state batteries: challenges and perspectives, Front. Mater. (2020) 1–5, https://doi.org/10.3389/fmats.2020.00111.
[4] K.J. Kim, M. Balaish, M. Wadaguchi, L. Kong, J.L.M. Rupp, Solid-State Li–metal batteries: challenges and horizons of oxide and sulfide solid electrolytes and their interfaces, Adv. Energy Mater. (2020) 2002689, https://doi.org/10.1002/aenm.202002689.
[5] H.-J. Deiseroth, S.-T. Kong, H. Eckert, J. Vannahme, C. Reiner, T. Zaiß, M. Schlosser, Li6PS5X: a class of crystalline li-rich solids with an unusually high Li + Mobility, Angew. Chem. Int. Ed. 47 (4) (2008) 755–758, https://doi.org/10.1002/anie.200703900.
[6] Y. Kato, S. Hori, T. Saito, K. Suzuki, M. Hirayama, A. Mitsui, M. Yonemura, H. Iba, R. Kanno, High-power all-solid-state batteries using sulfide superionic conductors, Nat. Energy 1 (4) (2016), https://doi.org/10.1038/nenergy.2016.30.
[7] S. Wang, R. Fang, Y. Li, Y. Liu, C. Xin, F.H. Richter, C.W. Nan, Interfacial challenges for all-solid-state batteries based on sulfide solid electrolytes, J. Mater. 7 (2) (2021) 209–218, https://doi.org/10.1016/j.jmat.2020.09.003.
[8] F. Marchini, B. Porcheron, G. Rousse, L. Albero Blanquer, L. Droguet, D. Foix, T. Koç, M. Deschamps, J.M. Tarascon, The hidden side of nanoporous β-Li3PS4 Solid Electrolyte, Adv. Energy Mater. 11 (34) (2021) 2101111, https://doi.org/10.1002/aenm.202101111.
[9] Y. Zhu, X. He, Y. Mo, Origin of outstanding stability in the lithium solid electrolyte materials: insights from thermodynamic analyses based on first-principles calculations, ACS Appl. Mater. Interfaces 7 (42) (2015) 23685–23693, https://doi.org/10.1021/acsami.5b07517.
[10] C. Cao, Z.-B. Li, X.-L. Wang, X.-B. Zhao, W.-Q. Han, Recent advances in inorganic solid electrolytes for lithium batteries, Front. Energy Res. (2014).
[11] P. Hartmann, T. Leichtweiss, M.R. Busche, M. Schneider, M. Reich, J. Sann, P. Adelhelm, J. Janek, Degradation of NASICON-type materials in contact with lithium metal: formation of mixed conducting interphases (MCI) on solid electrolytes, J. Phys. Chem. C. 117 (41) (2013) 21064–21074, https://doi.org/10.1021/jp4051275.
[12] S. Wenzel, T. Leichtweiss, D. Krüger, J. Sann, J. Janek, Interphase formation on lithium solid electrolytes - an in situ approach to study interfacial reactions by photoelectron spectroscopy, Solid State Ion.-. 278 (2015) 98–105, https://doi.org/10.1016/j.ssi.2015.06.001.
[13] S. Wenzel, Justus Liebig University Giessen. Thermodynamic and Kinetic Instability of Inorganic Solid Electrolytes at Lithium and Sodium Metal Electrodes, Universitätsbibliothek Gießen, 2016, https://doi.org/10.22029/JLUPUB-10375.
[14] Y. Xiao, Y. Wang, S.-H. Bo, J.C. Kim, L.J. Miara, G. Ceder, Understanding interface stability in solid-state batteries, Nat. Rev. Mater. 5 (2020) 105–126, https://doi.org/10.1038/s41578-019-0157-5.
[15] X. Meng, X.-Q. Yang, X. Sun, Emerging applications of atomic layer deposition for lithium-ion battery studies, Adv. Mater. 24 (2012) 3589–3615, https://doi.org/10.1002/adma.201200397.
[16] M. Hallot, B. Caja-Munoz, C. Leviel, O.I. Lebedev, R. Retoux, J. Avila, P. Roussel, M.C. Asensio, C. Lethien, Atomic layer deposition of a nanometer-thick Li_3PO_4 protective layer on $LiNi_{0.5}Mn_{1.5}O_4$ films: dream or reality for long-term cycling ? ACS Appl. Mater. Interfaces 13 (2021) 15761–15773, https://doi.org/10.1021/acsami.0c21961.
[17] M. Létiche, E. Eustache, J. Freixas, A. Demortière, V. De Andrade, L. Morgenroth, P. Tilmant, F. Vaurette, D. Troadec, P. Roussel, T. Brousse, C. Lethien, Atomic layer deposition of functional layers for on chip 3D Li-ion all solid state microbattery, Adv. Energy Mater. 7 (2017) 1601402, https://doi.org/10.1002/aenm.201601402.
[18] A. Kato, A. Hayashi, M. Tatsumisago, Enhancing Utilization of Lithium Metal Electrodes in All-Solid-State Batteries by Interface Modification with Gold Thin Films, J. Power Sources 309 (2016) 27–32, https://doi.org/10.1016/j.jpowsour.2016.01.068.
[19] F. Deng, Y. Wu, W. Tang, S. Song, Z. Wen, M. Kotobuki, L. Lu, J. Yao, N. Hu, J. Molenda, Conformal, nanoscale γ-Al2O3 coating of garnet conductors for solid-state lithium batteries, Solid State Ion.-. 342 (2019) 115063, https://doi.org/10.1016/j.ssi.2019.115063.
[20] J. Cui, J.H. Kim, S. Yao, A. Guerfi, A. Paolella, J.B. Goodenough, H. Khani, Exploration of metal alloys as zero-resistance interfacial modification layers for garnet-type solid electrolytes, Adv. Funct. Mater. 33 (10) (2023), https://doi.org/10.1002/adfm.202210192.
[21] A.L. Santhosha, L. Medenbach, J.R. Buchheim, P. Adelhelm, The indium−lithium electrode in solid-state lithium-ion batteries: phase formation, redox potentials, and interface stability, Batter Supercaps 2 (6) (2019) 524–529, https://doi.org/10.1002/batt.201800149.
[22] S. Wenzel, S. Randau, T. Leichtweiß, D.A. Weber, J. Sann, W.G. Zeier, J. Janek, Direct observation of the interfacial instability of the fast ionic conductor Li10GeP2S12 at the lithium metal anode, Chem. Mater. 28 (7) (2016) 2400–2407, https://doi.org/10.1021/acs.chemmater.6b00610.
[23] S. Wenzel, D.A. Weber, T. Leichtweiss, M.R. Busche, J. Sann, J. Janek, Interphase formation and degradation of charge transfer kinetics between a lithium metal anode and highly crystalline Li7P3S11 Solid Electrolyte, Solid State Ion.-. 286 (2016) 24–33, https://doi.org/10.1016/j.ssi.2015.11.034.
[24] S. Wenzel, S.J. Sedlmaier, C. Dietrich, W.G. Zeier, J. Janek, Interfacial reactivity and interphase growth of argyrodite solid electrolytes at lithium metal electrodes, Solid State Ion.-. 318 (2018) 102–112, https://doi.org/10.1016/j.ssi.2017.07.005.
[25] J.S. Gibson, S. Narayanan, J.E.N. Swallow, P. Kumar-Thakur, M. Pasta, T.L. Lee, R. S. Weatherup, Gently does it!: in situ preparation of alkali metal-solid electrolyte interfaces for photoelectron spectroscopy, Faraday Discuss. 236 (2022) 267–287, https://doi.org/10.1039/d1fd00118c.
[26] K.N. Wood, K.X. Steirer, S.E. Hafner, C. Ban, S. Santhanagopalan, S.H. Lee, G. Teeter, Operando X-ray photoelectron spectroscopy of solid electrolyte interphase formation and evolution in Li2S-P2S5 solid-state electrolytes, Nat. Commun. 9 (1) (2018), https://doi.org/10.1038/s41467-018-04762-z.
[27] S. Narayanan, U. Ulissi, J.S. Gibson, Y.A. Chart, R.S. Weatherup, M. Pasta, Effect of current density on the solid electrolyte interphase formation at the lithium|Li6PS5Cl interface, Nat. Commun. 13 (1) (2022), https://doi.org/10.1038/s41467-022-34855-9.
[28] A. Schwöbel, R. Hausbrand, W. Jaegermann, Interface Reactions between LiPON and lithium studied by in-situ x-ray photoemission, Solid State Ion.-. 273 (2015) 51–54, https://doi.org/10.1016/j.ssi.2014.10.017.
[29] T. Koç, F. Marchini, G. Rousse, R. Dugas, J.-M. Tarascon, Search of the best solid electrolyte-layered oxide pairing for assembling practical all-solid-state batteries, ACS Appl. Energy Mater. 4 (2021) 13575–13585, https://doi.org/10.1021/acsaem.1c02187.
[30] J.P. Rueff, J.M. Ablett, D. Céolin, D. Prieur, T. Moreno, V. Balédent, B. Lassalle-Kaiser, J.E. Rault, M. Simon, A. Shukla, The GALAXIES beamline at the SOLEIL synchrotron: inelastic x-ray scattering and photoelectron spectroscopy in the hard x-ray range, J. Synchrotron Radiat. 22 (1) (2015) 175–179, https://doi.org/10.1107/S160057751402102X.
[31] S. Tanuma, C.J. Powell, D.R. Penn, Calculations of electron inelastic mean free paths. IX. Data for 41 elemental solids over the 50 eV to 30 keV range, Surf. Interface Anal. 43 (2011) 689–713, https://doi.org/10.1002/sia.3522.
[32] A. Kato, H. Kowada, M. Deguchi, C. Hotehama, A. Hayashi, XPS and SEM Analysis between Li / Li 3 PS 4 interface with Au Thin Fi Lm for all- solid-state lithium batteries, Solid State Ion.-. 322 (2018) 1–4, https://doi.org/10.1016/j.ssi.2018.04.011.
[33] K. Wissel, L.M. Riegger, C. Schneider, A.I. Waidha, T. Famprikis, Y. Ikeda, B. Grabowski, R.E. Dinnebier, B.V. Lotsch, J. Janek, W. Ensinger, O. Clemens, Dissolution and Recrystallization Behavior of Li3PS4 in Different Organic Solvents

with a Focus on N-Methylformamide, ACS Appl. Energy Mater. 6 (15) (2023) 7790–7802, https://doi.org/10.1021/acsaem.2c03278.
[34] J. Auvergniot, A. Cassel, J.-B. Ledeuil, V. Viallet, V. Seznec, R. Dedryvère, Interface Stability of Argyrodite Li_6PS_5Cl toward $LiCoO_2$, $LiNi_{1/3}Co_{1/3}Mn_{1/3}O_2$, and $LiMn_2O_4$ in Bulk All-Solid-State Batteries, Chem. Mater. 29 (2017) 3883–3890, https://doi.org/10.1021/acs.chemmater.6b04990.
[35] K.N. Wood, K.X. Steirer, S.E. Hafner, C. Ban, S. Santhanagopalan, S.H. Lee, G. Teeter, Operando X-ray photoelectron spectroscopy of solid electrolyte interphase formation and evolution in Li2S-P2S5 Solid-State Electrolytes, Nat. Commun. 9 (1) (2018) 1–10, https://doi.org/10.1038/s41467-018-04762-z.
[36] X.S. Zhang, J. Wan, Z.Z. Shen, S.Y. Lang, S. Xin, R. Wen, Y.G. Guo, L.J. Wan, Situ analysis of interfacial morphological and chemical evolution in all-solid-state lithium-metal batteries, Angew. Chem. - Int. Ed. (2024), https://doi.org/10.1002/anie.202409435.
[37] R. Dedryvère, S. Laruelle, S. Grugeon, P. Poizot, D. Gonbeau, J.-M. Tarascon, Contribution of X-ray photoelectron spectroscopy to the study of the electrochemical reactivity of CoO toward lithium, Chem. Mater. 16 (2004) 1056–1061, https://doi.org/10.1021/cm0311269.
[38] M. Calpa, N.C. Rosero-Navarro, A. Miura, R. Jalem, Y. Tateyama, K. Tadanaga, Chemical stability of Li4PS4I solid electrolyte against hydrolysis, Appl. Mater. Today 22 (2021) 100918, https://doi.org/10.1016/j.apmt.2020.100918.
[39] L. Pérez Ramírez, F. Bournel, J.-J. Gallet, L. Dudy, F. Rochet, Testing the cabrera–mott oxidation model for aluminum under realistic conditions with near-ambient pressure photoemission, J. Phys. Chem. C. (2022) acs.jpcc.1c09388, https://doi.org/10.1021/acs.jpcc.1c09388.
[40] S. Hao, C. Wolverton, Lithium transport in amorphous Al_2O_3 and AlF_3 for discovery of battery coatings, J. Phys. Chem. C. 117 (2013) 8009–8013, https://doi.org/10.1021/jp311982d.
[41] J.S. Park, X. Meng, J.W. Elam, S. Hao, C. Wolverton, C. Kim, J. Cabana, Ultrathin lithium-ion conducting coatings for increased interfacial stability in high voltage lithium-ion batteries, Chem. Mater. 26 (10) (2014) 3128–3134, https://doi.org/10.1021/cm500512n.
[42] A.L. Davis, R. Garcia-Mendez, K.N. Wood, E. Kazyak, K.-H. Chen, G. Teeter, J. Sakamoto, N.P. Dasgupta, Electro-chemo-mechanical evolution of sulfide solid electrolyte/Li metal interfaces: operando analysis and ALD interlayer effects, J. Mater. Chem. A 8 (2020) 6291–6302, https://doi.org/10.1039/C9TA11508K.
[43] Z.D. Hood, A.U. Mane, A. Sundar, S. Tepavcevic, P. Zapol, U.D. Eze, S.P. Adhikari, E. Lee, G.E. Sterbinsky, J.W. Elam, J.G. Connell, Multifunctional coatings on sulfide-based solid electrolyte powders with enhanced processability, stability, and performance for solid-state batteries, Adv. Mater. 35 (2023) 2300673, https://doi.org/10.1002/adma.202300673.
[44] I.A. Sokolov, N.A. Valova, Y.P. Tarlakov, A.A. Pronkin, Electrical properties and the structure of glasses in the Li_2SO_4-$LiPO_3$ System, Glass Phys. Chem. 29 (2003) 548–554, https://doi.org/10.1023/B:GPAC.0000007930.11101.ee.
[45] H. Ishii, K. Sugiyama, E. Ito, K. Seki, Energy level alignment and interfacial electronic structures at organic/metal and organic/organic interfaces, Adv. Mater. 11 (1999) 605.
[46] S. Doniach, M. Sunjic, Many-electron singularity in x-ray photoemission and x-ray line spectra from metals, J. Phys. C Solid State Phys. 3 (2) (1970) 285, https://doi.org/10.1088/0022-3719/3/2/010.
[47] J. Konys, H.U. Borgstedt, The product of the reaction of alumina with lithium metal, J. Nucl. Mater. 131 (2–3) (1985) 158–161, https://doi.org/10.1016/0022-3115(85)90454-4.
[48] R.S. Negi, Y. Yusim, R. Pan, S. Ahmed, K. Volz, R. Takata, F. Schmidt, A. Henss, M. T. Elm, A Dry-Processed Al2O3/LiAlO2 coating for stabilizing the cathode/electrolyte interface in high-ni ncm-based all-solid-state batteries, Adv. Mater. Interfaces 9 (8) (2022), https://doi.org/10.1002/admi.202101428.
[49] L. Dahéron, R. Dedryvère, H. Martinez, D. Flahaut, M. Ménétrier, C. Delmas, D. Gonbeau, Possible explanation for the efficiency of al-based coatings on LiCoO2: surface properties of LiCo1-xAlxO2 Solid Solution, Chem. Mater. 21 (2009) 5607–5616, https://doi.org/10.1021/cm901972e.